Intramolecular Polarization Induces Electron–Hole Charge Separation in Light-Harvesting Molecular Triads

ARTICLE *in* THE JOURNAL OF PHYSICAL CHEMISTRY C · DECEMBER 2013

Impact Factor: 4.77 · DOI: 10.1021/jp408955e

4 AUTHORS, INCLUDING:

L. G. C. Rego
Federal University of Santa Catarina
58 PUBLICATIONS **1,429** CITATIONS
SEE PROFILE

K. T. Mazon
Federal University of Santa Catarina
24 PUBLICATIONS **98** CITATIONS
SEE PROFILE

Jan-Ole Joswig
Technische Universität Dresden
65 PUBLICATIONS **588** CITATIONS
SEE PROFILE

THE JOURNAL OF PHYSICAL CHEMISTRY C

Article

pubs.acs.org/JPCC

Intramolecular Polarization Induces Electron–Hole Charge Separation in Light-Harvesting Molecular Triads

Luis G. C. Rego,*[,†] Bruno C. Hames,[†] Kahio T. Mazon,[†] and Jan-Ole Joswig[‡]

[†]Department of Physics, Universidade Federal de Santa Catarina, Florianópolis, SC 88040-900,Brazil

[‡]Physikalische Chemie, Technische Universität Dresden, 01062 Dresden, Germany

Supporting Information

ABSTRACT: Artificial light-harvesting supramolecular structures reproduce the light-to-electrochemical energy transduction mechanisms observed in natural photosynthesis. Among them the prototypical carotenoid(C)–porphyrin(P)–fullerene(C_{60}) type of structures have been the most studied. Several experiments performed in such structures, and others alike, have shown that the photoexcited state $C-\ ^1P-C_{60}$ decays to the metastable charge-separated state $C-\ P^{\bullet+}\ -C_{60}^{\bullet-}$ within a few picoseconds, whereas the final charge-separated state, $C^{\bullet+}-\ P\ -C_{60}^{\bullet-}$, is obtained within hundreds of picoseconds. This paper introduces a nonlinear polarizable extended Hückel Hamiltonian that describes the charge dynamics and charge-separation effects in such triads by means of quantum dynamics simulations performed on the photoexcited electron–hole pair. The results are interpreted on the basis of the discrete self-trapping equation and enlighten the role played by the polarizability on charge-separation phenomena.

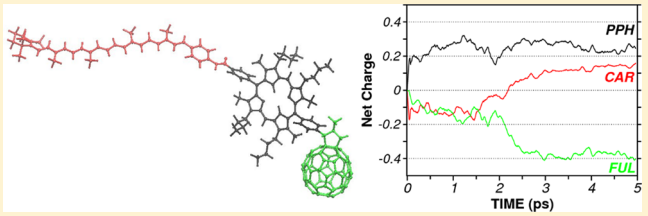

1. INTRODUCTION

The quantum dynamics that controls energy and charge-transfer processes in large molecular structures is fundamental for a variety of phenomena, including solar energy conversion in organic solar cells, natural and artificial photosynthesis, electron transfer in proteins, among others. Of particular interest nowadays are light-harvesting and energy transduction processes in supramolecular structures and hybrid photosynthetic systems.[1−5] Nature has developed a sophisticated molecular-based energy conversion system, in which electron transfer processes play a major role.[5,6] It is believed that the knowledge obtained with the understanding of such underlying molecular processes can be used to devise the next generation of solar cell devices.[7−10] Studies of the initial energy transfer processes in photosynthesis date back from the 1950s, when the flash photolysis technique was applied to study the problem.[11] Later in the 1970s, Porter,[12] and independently Alfano and Shapiro,[13] pioneered the use of picosecond time-resolved spectroscopy to investigate energy transfer in antenna systems.[13] Nowadays, femtosecond electronic spectroscopy is used to investigate, among other issues, the role of quantum coherences for light harvesting in antenna complexes.[4] A pioneering research program aimed at understanding and synthesizing artificial photosynthetic supramolecular structures has been undertaken by the Center for the Study of Early Events in Photosynthesis. The group has synthesized a family of carotenoid(C)–porphyrin(P)–fullerene(C_{60}) molecular triads[1,2,14] and characterized its energy and charge-transfer events, from photoexcitation to fluorescence. Several other groups have also performed time-resolved optical experiments in different light-harvesting systems.[14,15] Nevertheless, the $C-P-C_{60}$ type of structures remain the most studied of all.[16−19] Some studies report that upon photoexcitation to state $C-\ ^1P-C_{60}$, the system decays to the metastable charge-separated state $C-\ P^{\bullet+}\ -C_{60}^{\bullet-}$ within a few picoseconds, with almost unity quantum efficiency.[1,2] The final charge-separated state, $C^{\bullet+}-\ P\ -C_{60}^{\bullet-}$ is obtained within hundreds of picoseconds, with a quantum yield that reaches 90% in polar solutions at room temperature. Similar relaxation times have been measured for several other fullerene–porphyrin-based systems.[14,20,21] Experiments also evidence that solvation effects—particularly its polarity—are not the determining factor for the first charge-separation event; however, the $C^{\bullet+}-\ P\ -C_{60}^{\bullet-}$ state is not observed in nonpolar solvents like toluene.[22−24]

Recently, the photoinduced charge-separation dynamics in a $C-P-C_{60}$ triad was given another description, based on femtosecond time-resolved optical spectroscopy measurements and quantum dynamical simulations performed within the time-dependent density functional theory (TDDFT),[25] both limited to the earliest 100 fs dynamics after photoexcitation. This combined study reports that the primary charge-separation event, which yields the state $C-\ P^{\bullet+}\ -C_{60}^{\bullet-}$, takes place within 70 fs, driven by the coherent dynamics of electrons and ions in the triad. However, the conclusion of the recent study differs from previous measurements carried out on the same *meso*-tetraarylporphyrin triad,[2] which evidenced a photoinduced electron transfer to the fullerene in 32 ps. For such type of systems—based on the porphyrin–fullerere dyad struc-

Received: September 6, 2013
Revised: December 8, 2013
Published: December 11, 2013

   dx.doi.org/10.1021/jp408955e | *J. Phys. Chem. C* 2014, 118, 126−134

ture[1,2,14,15,20,21,24] and multiporphyrin arrays[3]—transient spectroscopic methods have revealed evidence of the charge-separated state formation ranging from 3 ps to approximately 40 ps.

The endeavor of simulating the quantum dynamics of energy and charge-transfer processes in large molecular structures and under realistic conditions has only recently been accomplished within the atomistic framework. The problem can be simplified at two limiting regimes though.[26,27] In the case of weak electronic donor−acceptor coupling, when the thermodynamic driving force and the influence of the environment are both paramount, the formalisms derived from the Marcus Theory can be applied. On the other limit, where the electronic coupling between the donor and acceptor states of the system is strong, it is possible to simplify the problem by using the time-dependent Schrödinger equation for the quantum system with the effects of the environment included perturbatively, if necessary at all. The investigation undertaken herein is more difficult to describe because the effect lies midway between these simplifying limits.

The paper introduces a phenomenological Hamiltonian that can account for the charge dynamics and charge-separation effect in the $C-P-C_{60}$ triads. Two dynamical regimes are revealed for the electron−hole pair: a transient oscillatory behavior and the nonlinear self-trapping regime. The study also enlightens the role played by the intramolecular polarizability on the charge-separation effect in supramolecular structures. The results are described in the framework of the self-trapping nonlinear Schrödinger equation (NLSE), which is well-known for describing self-trapping phenomena observed in confined Bose−Einstein condensates at low temperatures,[28−31] solitonic wave propagation in nonlinear media,[32] polaron dynamics,[33] and localization of vibrational energy in molecular systems,[34] among others.[36] In regard to our simulations, the self-trapping of the electron wavepacket is driven by the nonlinear polarizable Hückel Hamiltonian, which is observed around 2 ps, after an initial charge delocalization from the porphyrin chromophore that occurs in ∼100 fs. Quantum dynamics simulations were performed for $C-P-C_{60}$ triads comprised of porphyrins with different substituents, along with nuclear dynamics at room temperature. Although charge separation tends to occur for both simulation cases, the effect occurs with less efficiency as the macrocycle becomes more flexible, as in the case of meso-substituted-tetraaryl porphyrins. The simulation results corroborate the experimental studies that report the formation of charge-separated states within a few picoseconds for this family of molecular triads and several other supramolecular structures.[1,2,14,15,20,21]

2. THEORY AND METHODS

The electronic quantum dynamics simulations were performed with a semiempirical molecular orbital method developed for large scale systems. Classical molecular dynamics and electronic quantum dynamics methods were combined sequentially in a computational method that has been used for studying charge-transfer processes in a variety of molecular systems. Some details of the theoretical approach, which are relevant for the present problem, are described below; general details can be found in previous publications.[38−40]

For preparing the molecular structure of the triad, prior to the electron−hole quantum dynamics simulations, the $C-P-C_{60}$ was submitted to a molecular dynamics (MD) procedure in the canonical NVT ensemble at 300 K for 15 ps in the gas phase. Then, after the thermal equilibration, MD production runs were carried out for 5 ps in the microcanonical NVE ensemble. The NVT molecular dynamics calculations have the goal of producing an initial molecular conformation that is typical for the ambient temperature because the molecular geometry gained just by minimizing the ground state (GS) energy is unrealistic for the triad and does not provide a good initial configuration. The NVE ensemble, which is more consistent with a simulation in the gas phase, is carried out to generate the nuclear dynamics upon which the electronic wavepackets will be propagated. Such short time interval molecular frames convey nuclear dynamics effects into the electronic quantum dynamics; our simulations reveal that temperature effects are relevant for a better charge-separation process because thermal effects take the system out of metastable states. These Born−Oppenheimer molecular-dynamics simulations were performed with the density functional tight-binding (DFTB) method[41−43] in the self-consistent charge (SCC) extension.[44] This method uses a minimal valence basis set and considers only one- and two-center integrals to set up the Hamiltonian matrix. Calculations of the excitation spectra have been performed using a linear-response extension to the DFTB method[45] (Supporting Information).

The electronic structure of the system is described through a tight-binding Hamiltonian based on the semiempirical Extended Hückel Theory (EHT).[46] The EHT method is well-suited to be applied to large systems and provides valuable insights on the role of chemical bonding and molecular conformation dynamics. Thus, upon the EHT Hamiltonian, additional long-range interaction terms can be included, such as the interaction with an atomistic dielectric environment.[38,39,47] The matrix elements of the plain EHT describe the effects associated with the chemical bonding as $H^0_{ij}(t) = K_{ij}S_{ij}(t)[E_i+E_j]/2$, where K_{ij} is the modified Wolfsberg−Helmholz parameter,[48] $S_{ij}(t)$ is the time-dependent overlap matrix between diabatic Slater-type atomic orbitals (STO), and the diagonal elements, $H^0_{ii} = E_i$, correspond to the valence ionization potentials of a given atomic species.

To build up the Hamiltonian, both the electron and the hole wavepackets are written as a linear combination of STO orbitals, $|\Psi^{El}\rangle = \Sigma_i C_i^{El}(t)|i(t)\rangle$ and $|\Psi^{Hl}\rangle = \Sigma_i C_i^{Hl}(t)|i(t)\rangle$, with complex coefficients C^{El} and C^{Hl} to account for the quantum dynamics of the wavepackets.

The intramolecular electronic polarization induced in the system by the presence of the photoexcited electron−hole pair is essential to stabilize the charge-separated state in the triad; formally, this is accomplished by including a local nonlinear mean-field potential to the Hückel Hamiltonian $H^0(t)$. The effect is included in the formalism by the charge induced-dipole coupling mechanism. If there is a charge perturbation on the molecule, for instance caused by the photoexcitation of the molecule or by the transfer of an electron into the molecule, it produces on the k-th atomic site a local field $\vec{E}_k = \Sigma_{l\neq k}(q_l^{Hl} - q_l^{El})(\vec{r}_k - \vec{r}_l)/|\vec{r}_k - \vec{r}_l|^3$, where q_l^{El} and q_l^{Hl} are given by the Mulliken local charges on atom l due to the photoexcited electron and hole wavepackets

$$q = e\mathrm{Re}\Big[\sum_i^{\mathrm{atom}} \sum_j S_{ij}(t)C_i^*(t)C_j(t)\Big] \tag{1}$$

The induced-dipole moment $\vec{p}_k$ can be written in the linear response approximation as

dx.doi.org/10.1021/jp408955e | J. Phys. Chem. C 2014, 118, 126−134

$$\vec{p}_k = \sum_{l\neq k} \alpha_{kl}\vec{E}_{kl} = \sum_{l\neq k} [\alpha_k^0 \int_0^{r_l} R_n^2(r) r^2 dr] \frac{(\vec{r}_k - \vec{r}_l)}{|\vec{r}_k - \vec{r}_l|^3} (q_l^{Hl} - q_l^{El}) \tag{2}$$

The term α_k^0 is the scalar atomic polarizability of the k-th atom,[49] and α_{kl} is defined to produce a distance-dependent atomic polarizability that vanishes as $r_l \rightarrow r_k$,

$$\alpha_{kl} = \alpha_k^0 \int_0^{r_l} R_n^2(r) r^2 dr \tag{3}$$

where $R_n(r) = (2\zeta)^{n+1/2}\ (1/(2n)!)^{1/2}\ r^{n-1}e^{-\zeta r}$ is the normalized radial part of the Slater-type atomic orbital with principal quantum number n, and r_l is the distance between atoms l and k. The potential produced by all the induced atomic dipoles in the molecule is given by

$$V^{\mathrm{DP}}(\vec{r}) = \sum_k \frac{\vec{p}_k \cdot (\vec{r} - \vec{r}_k)}{|\vec{r} - \vec{r}_k|^3} \tag{4}$$

$$= \sum_l \left[\sum_{k\neq l} \alpha_k^0 \frac{(\vec{r} - \vec{r}_k)\cdot(\vec{r}_k - \vec{r}_l)}{|\vec{r} - \vec{r}_k|^3 |\vec{r}_k - \vec{r}_l|^3} \int_0^{r_l} R_n^2(r) r^2 dr \right] (q_l^{Hl} - q_l^{El}) \tag{5}$$

The resulting potential decays as $\sim$ (1/distance).[4] Matrix elements for the potential can be obtained by expanding $V^{\mathrm{DP}}(\vec{r})$ around the midpoint of two atomic centers, $\vec{r}_0 = (\vec{r}_i + \vec{r}_j)/2$, as

$$V_{ij}^{\mathrm{DP}} \approx \langle i | [V^{\mathrm{DP}}(\vec{r}_0) + \vec{\nabla} V^{\mathrm{DP}}(\vec{r}_0)(\vec{r} - \vec{r}_0)] | j \rangle$$
$$\approx V^{\mathrm{DP}}(\vec{r}_0) S_{ij} + \vec{\nabla} V^{\mathrm{DP}}(\vec{r}_0) \left[\frac{1}{e}\vec{\mu}_{ij} - \vec{r}_0 S_{ij} \right] \tag{6}$$

where $S_{ij} = \langle i | j \rangle$ is the overlap matrix element and $\vec{\mu}_{ij} = e\langle i | \vec{r} | j \rangle$ is the transition dipole matrix element between atomic orbitals $|i\rangle$ and $|j\rangle$. Carrying out the calculations of eq 6, one obtains the following expression for the matrix element of the intramolecular induced polarization potential

$$V_{ij}^{\mathrm{DP}} \approx \frac{1}{4\pi\varepsilon_0} \sum_k \left[S_{ij}(\vec{r}_0 - \vec{r}_k) - 2\left(\frac{1}{e}\vec{\mu}_{ij} - S_{ij}\vec{r}_0 \right) \right] \cdot \frac{\vec{p}_k}{|\vec{r}_0 - \vec{r}_k|^3} \tag{7}$$

To avoid numerical divergences in eq 7, which occur when a dipole moment $\vec{p}_k$ is found at the midpoint of orbitals $|i\rangle$ and $|j\rangle$, that is, $\vec{r}_k = \vec{r}_0$, a cutoff radius of $\sim$2.5 Å is adopted, so that $V_{ij}^{\mathrm{DP}} = 0$ for $|\vec{r}_0 - \vec{r}_k| \leq r_{\mathrm{cut}}$ and V_{ij}^{DP} is given by eq 7 otherwise. The cutoff radius was also chosen to eliminate nearest-neighbor couplings through the induced-dipole potential—the approximate C−C distance in the structure is 1.4 Å—because the model assumes that all short-range interactions are described by the Hückel Hamiltonian $H^0(t)$. The conclusions are robust against small changes of this value (up to ±0.5 Å).

The total Hamiltonian is now composed of the matrix elements $H_{ij}(t) = H_{ij}^0(t) + V_{ij}^{\mathrm{DP}}(t)$, in the STO basis. Notice that the induced-dipole potential introduces a local nonlinearity to the original Hückel Hamiltonian. From the formal viewpoint, the ensuing Hamiltonian leads to a self-trapping nonlinear Schrödinger equation (NLSE) that is equivalent to[33,34,36]

$$i\hbar \frac{d\mathbf{SC}}{dt} = H_0\mathbf{C} + \eta \boldsymbol{F}(|\mathbf{C}|^2)\mathbf{C} \tag{8}$$

which was introduced to describe self-trapping of vibrational energy[34] as well as polarons in molecular systems.[33,36] The time-dependent polarizable Hückel equation is formally analogous to eq 8, where $\boldsymbol{S}$ is the overlap matrix and $\boldsymbol{C}$ = col $(C_1, C_2, \ldots, C_n)$ is a complex n-component vector that describes the electron and hole wavepackets, H_0 is the symmetric Hückel Hamiltonian matrix, and $\eta \boldsymbol{F}(|\mathbf{C}|^2)$ is the nonlinear self-trapping potential produced by the induced polarization. In particular, η is referred to as the nonlinearity parameter; it induces the self-trapping effect when its value is above a critical value η_c, which is system dependent. According to our studies, the self-trapping effect produced by the nonlinear polarizable Hückel Hamiltonian is responsible for the charge-separation process because the electron is trapped in the fullerene fragment and dissociates from the hole wavepacket. More information about the NLSE can be found in the Supporting Information.

Regarding the quantum dynamics propagation of the photoexcited electron−hole pair, the initial wavepackets are assigned to the frontier molecular orbitals (MO) of the chromophore moiety (the porphyrin moiety, PPH). They are initially described as $|\Psi(0)\rangle = \Sigma_i^{\mathrm{PPH}} C_i(0)|i(0)\rangle$, with $\mathbf{C}(0)$ gained from $H_{\mathrm{PPH}}C^{\varepsilon} = \varepsilon S_{\mathrm{PPH}}C^{\varepsilon}$. We performed simulations considering two distinct types of initial conditions for the system: in one case, the system is initially set with the electron on the lowest unoccupied molecular orbital (LUMO) and the hole on the highest occupied molecular orbital (HOMO) of the PPH fragment; the other initial condition (results described in Supporting Information) is set with the electron described by a linear combination of the LUMO and LUMO+1 states and likewise for the hole formed by the HOMO and HOMO-1. The charge-separation effect is equal in both cases, despite some minor differences during the transient oscillatory charge kinetics before charge separation.

In practice, the electronic quantum dynamics (QD) is performed in two stages. First the nuclear coordinates, $\vec{R}_n(t)$, are obtained from the MD simulations, carried out without taking into account the wavepacket propagation, to produce the time-dependent STO basis functions $|i(t)\rangle$. The time-dependent Hamiltonian $H_{ij}(t) = H_{ij}^0(t) + V_{ij}^{\mathrm{DP}}(t)$ is built up upon the basis functions $|i(t)\rangle$, taking into account the coefficients $C^{El}(t)$ and $C^{Hl}(t)$, and it is diagonalized for each time step to produce adiabatic molecular orbitals $|\phi(t)\rangle$ of the entire system. The time propagation of the wavepackets is carried out in the adiabatic (MO) basis set, but the transmission of wavepacket coefficients to the next time slice is done in the diabatic (AO) basis set to avoid numerical problems caused by level-crossing and accidental degeneracies between MOs. The quantum dynamics results presented herein were obtained with δt = 0.3 fs since it provided a good interplay between electronic and nuclear intrinsic dynamics. Because the molecular dynamics is calculated independently of the wavepacket propagation, the method does not describe coherent electron-nuclei vibrations. This is an important effect during the first hundreds of femtoseconds, particularly so for molecular systems.[37] The importance of the effect tends to diminish after 1−2 ps, which is the time necessary to distribute (relax) the excess energy of the photoexcited electron−hole pair. The details of the procedure are described elsewhere.[38,50]

As already mentioned here, and yet to be discussed in the next section, some sources for discrepancies with experimental results are: the absence of solvent, the assumption of instantaneous photoexcitation, the sequential MD prior to QD methodology, as well as the extended Hückel phenomenological framework. Therefore, we propose a qualitative explanation of the observed experimental events, with order of

dx.doi.org/10.1021/jp408955e | J. Phys. Chem. C 2014, 118, 126−134

magnitude agreement between simulation and experimental results, which still have significant uncertainties of their own.

3. RESULTS AND DISCUSSION

The chemical structure of a $C-P-C_{60}$ triad investigated in the paper is shown in Figure 1A, along with a typical geometry

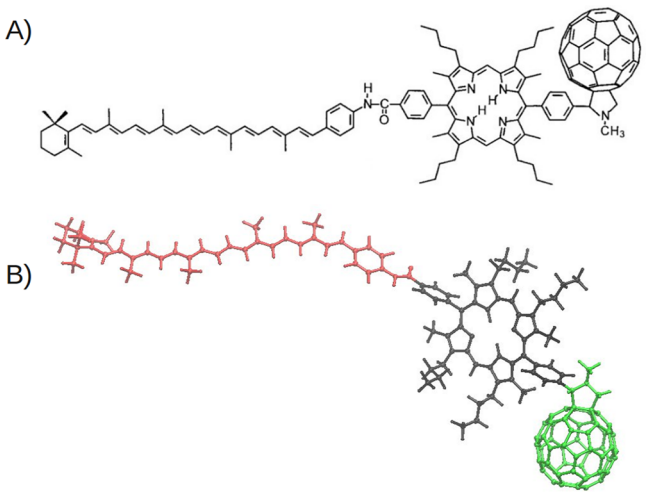

Figure 1. (A) Chemical structure of the $C-P-C_{60}$ triad investigated in the paper. (B) Typical geometry configuration obtained after MD thermalization in gas phase at 300K. Colors are used to identify the three components of the triad: the diaryloctaalkylporphoryn (black), the [60]fulleropyrrolidine (green), and the carotenoid tail (red), which are denoted by the labels PPH, FUL, and CAR, respectively.

configuration obtained from MD simulations at 300K, in gas phase, Figure 1B. Colors are used to identify the three components of the triad: the diaryloctaalkylporphoryn (black), the [60]fulleropyrrolidine (green), and the carotenoid tail (red), which are denoted by the labels PPH, FUL, and CAR, respectively. The size of the molecular structure presents a challenge for the theoretical simulations, which are regularly carried out in the gas phase. In some studies, calculations performed at the DFT[16,17] and TDDFT[18] levels of theory, along with our own performed using a linear-response extension to the DFTB method (Supporting Information), demonstrate that the absorption spectrum of the triad can be described as a combination from the spectra of each of the fragments, corroborating the findings of spectroscopy measurements. It is important to note, however, that at ambient conditions the triad is usually not found in the completely extended (linear) configuration that characterizes its ground state optmized geometry. It was shown by detailed molecular dynamics simulations in H_2O solution[19] that the free energy landscape is formed by several local minima of less than 1 k_BT; the resulting typical structures evince a twisted conformation like the one in Figure 1B. It has also been pointed out that solvation and entropic effects are particularly important for time scales of hundreds of picoseconds.[51] Nevertheless, to include the solvent in the simulation, for a long aspect ratio molecule such as the triad, thousands of solvent molecules are necessary[19] rendering the quantum mechanical calculations impractical. Based on experimental accounts,[22−24] we assume that it is reasonable to disregard the solvent effects for the early charge-separation event that occurs within 10 ps.

The study presented herein focuses on the first photoinduced charge-separation event that yields the metastable $C-P^{\bullet+}-C_{60}^{\bullet-}$ state. It has been demonstrated by numerous time-resolved measurements that the kinetics of this event is influenced by the substituent groups attached to the porphyrin cycle.[2,3,20,52] From the practical point of view, the choice of the substituent groups is made to ease the synthesis of the compound, by increasing its solubility and limiting aggregation of the triads. But they also determine the charge-transfer rates and the corresponding quantum yields of the processes. For instance, time-resolved absorption and emission measurements carried out on porphyrins with β-alkyl-substituents, such as those attached to the triad in Figure 1, show that the primary photoinduced electron transfer to the fullerene moiety occurs with a time constant in the range 3 ps $< \tau <$ 12 ps and unity quantum efficiency,[2] besides relative insensitivity to solvent and temperature conditions.[24] However, if aryl rings are attached to the *meso* positions of the free-base porphyrin, electron transfer times of ∼30−40 ps have been observed, with equally high quantum efficiencies.[2,20] The same charge-separation behavior has been evidenced in measurements performed with different light-harvesting systems, such as the $(ZnP)_3-ZnP-H_2P-C_{60}$ hexad, comprising a $(ZnP)_3-ZnP$ antenna structure covalently linked to a H_2P-C_{60} reaction center.[20,52] In this case, the photoinduced charge-separated state $(ZnP)_3-ZnP-H_2P^{\bullet+}-C_{60}^{\bullet-}$ is formed with a time constant of 3 or 25 ps, depending on whether the free-base porphyrin has, respectively, β-alkyl or *meso*-aryl substituents attached to it.

It is known that the porphyrin macrocycle is very flexible, and its conformational deformations are strongly influenced by the type and position of the substituents.[53−56] In fact, such different macrocycle conformations give rise to altered physicochemical properties that can dictate the biological functions of porphyrins. In this work, we performed MD simulations for triads comprising a diaryl-octaalkyl-porphyrin (Figure 1) and a *meso*-tetraaryl-porphyrin (Supporting Information), verifying that the latter macrocycle is appreciably more flexible, as evinced by studies reported elsewhere.[54,55,57] We also verified, by carrying out quantum dynamics simulations, that the more flexible type of porphyrin macrocycle gives rise to wider energy fluctuations that lead to inferior efficiency in the charge-separation process.

In the remainder, we describe the quantum dynamics simulations performed for the electron−hole pair initially set on the photoexcited porphyrin chromophore; vertical photoexcitation is assumed. The initial charge densities of the electron and hole wavepackets are illustrated in Figure 2, which correspond to the LUMO (red) and HOMO (blue) of the porphyrin, respectively. Results for wavepackets built up as a

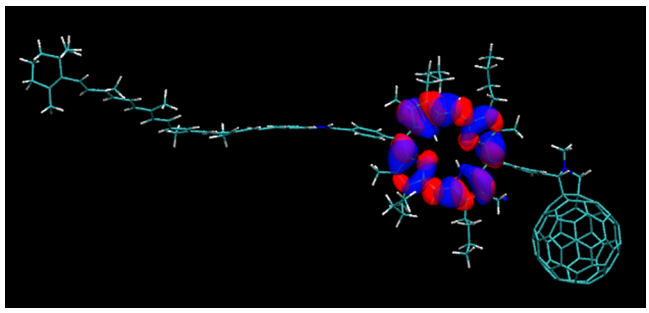

Figure 2. Charge densities of the photoexcited electron (red) and hole (blue) wavepackets, corresponding to the HOMO and LUMO molecular orbitals of the free-base porphyrin, respectively.

dx.doi.org/10.1021/jp408955e | J. Phys. Chem. C 2014, 118, 126−134

linear combination of frontier orbitals are presented as Supporting Information. Figure 3 shows simulation results of

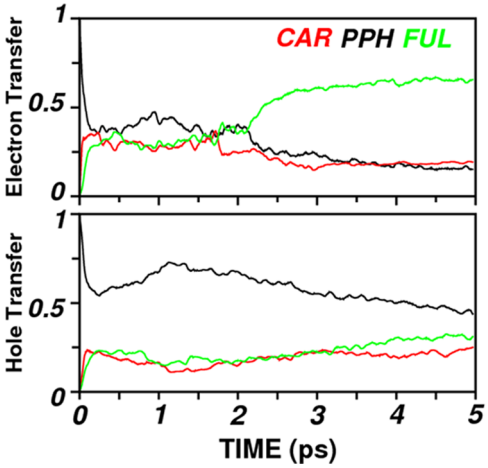

Figure 3. Time-dependent electron (A) and hole (B) wavepacket occupations on each of the fragments comprising the triad: carotene (CAR, in red), porphyrin (PPH, in black), and fullerene (FUL, in green). For guidance refer to Figure 1A.

the charge-transfer and charge-separation dynamics for the photoexcited electron and hole, as obtained by the quantum propagation method described in Section 2. The curves describe the time-dependent electron and hole wavepacket occupations on each of the triad's fragments: CAR, PPH, and FUL. The electron and hole wavepackets have very different dynamics. From the outset, the simulations evince three distinct dynamical regimes for the electron. Starting from the LUMO of the PPH moiety, the electron is scattered throughout the triad in ~100 fs. Similar behavior, though less intense, is also observed for the hole at this period. The charge dispersion at outset is driven by the combined effect of the initial electronic coupling among the fragments' molecular orbitals, by the polarization relaxation within the porphyrin fragment and by the nuclear motion. The electronic charge remains delocalized over the triad for approximately 2 ps, and then the electron density starts to build up into the FUL moiety until it is stabilized in that fragment. We ascribe this behavior to the self-trapping effect, which is produced by the nonlinear induced-dipole potential of the model's Hamiltonian. Together, the charge-induced intramolecular polarization field increases at the PPH–FUL junction (see Figure 5). The dynamics of the hole, however, proceeds independently of the electron trapping. We point out that the stabilizing effect of the induced polarization field quenches the large charge oscillations that occur when it is not included in the model.

Figure 4 shows the electron–hole net charge dynamics—defined as the difference between the hole (positive) and the electron (negative) wavepacket occupations—on the individual fragments of the triad. The curves exhibit a trend that was regularly observed in the simulations: the PPH fragment becomes positively charged throughout the simulation; part of the electronic charge is initially transferred to the CAR and FUL moieties from the porphyrin macrocycle; and eventually, electronic charge is transferred concomitantly from the CAR and PPH moieties to the FUL moiety (Supporting Information). Thus, the charge of the electronic wavepacket that is scattered through the triad migrates to the fullerene due to the self-trapping effect (Figure 3). On the basis of the

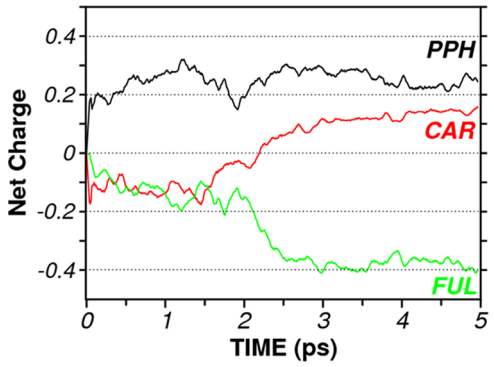

Figure 4. Time-dependent electron–hole net charge on each of the triad fragments: carotene (CAR, in red), porphyrin (PPH, in black), and fullerene (FUL, in green).

simulation results, we ascribe this irreversible charge transfer, driven by the self-trapping effect, to the decay of the photoexcited state $C-{}^1P-C_{60}$ and the formation of the metastable charge-separated state $C-P^{\bullet+}-C_{60}^{\bullet-}$ that is measured in the photochemical experiments with picosecond time resolution.[1,2,14,15,20,21] In addition, we believe that the high time-resolution pump–probe differential transmission spectra obtained for time delays t < 300 fs of the probe[25,58]—in particular, the transient photobleaching signal centered around the Q-band absorption resonance of the porphyrin moiety—can be associated to the initial charge relaxation effect shown in Figure 3.

The development and the dynamics of the induced polarization is shown through the panels of Figure 5, at the times t = 0, 0.1, 1.7, 2.0, 3.3, and 5 ps. The images show the intensity of the induced-dipole field, ranging from the unpolarized (red) to the very polarized (blue); white is moderately polarized. Since the induced polarization is produced by the presence of the photoexcited electron–hole pair, at t = 0, only the atoms of the PPH moiety are polarized (colors blue and white). During the transient scattering period, the polarization field oscillates and rotates mostly in the porphyrin cycle, until it reaches the neighboring FUL fragment ~t = 2.0 ps. The figures indicate that some of the induced polarization, between the PPH and FUL moieties, occur through space. Though the polarization field quickly oscillates into the CAR and FUL moieties during the scattering period, it does not stabilize fully in the CAR fragment. It does so, however, at the PPH–FUL junction, when enough electronic charge is transferred to the FUL. The effect increases as more charge is transferred to that moiety, as a consequence of the nonlinear nature of the polarizability. Simulations starting from a linear combination of frontier MOs [HOMO ± 1, LUMO ± 1] show the same behavior. Therefore, we conclude that the first charge-separation event in the $C-P-C_{60}$ triad is produced by the self-trapping of the electron in the *N*-methylfullero-pyrrolidine (MPC_{60}).

Figure 6 shows the density of states (DOS) for the triad, calculated for the molecular conformation at t = 0, with its HOMO located at −11.12 eV. From top to bottom, the graphs show the total DOS (blue) and its projection on the FUL (green), PPH (black), and CAR (red) moieties. Some molecular orbitals are shared between the neighboring pairs of fragments: CAR–PPH (for instance at −8.92, −9.23, −9.37, and −9.58 eV) and PPH–FUL (−8.45 and −8.3 eV). In particular, the electronic resonances between the frontier

dx.doi.org/10.1021/jp408955e | J. Phys. Chem. C 2014, 118, 126–134

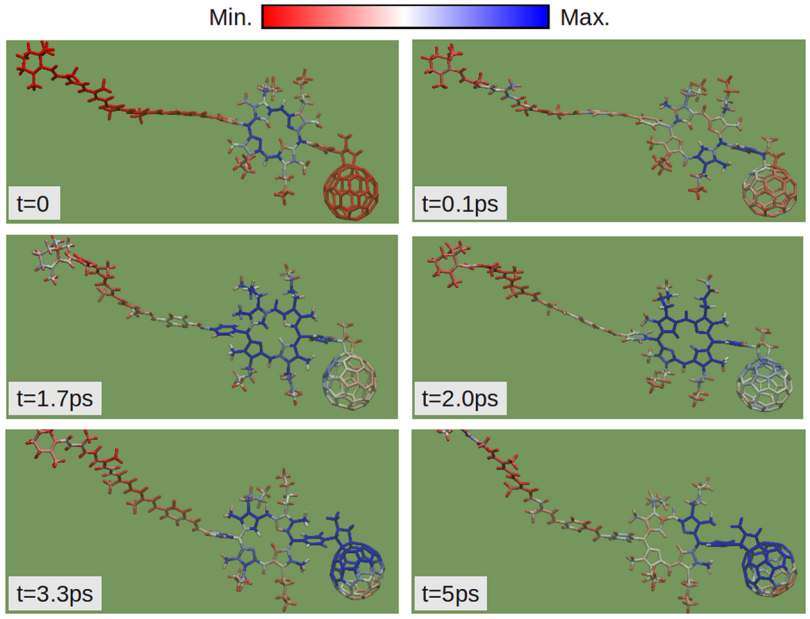

Figure 5. Intensity plot of the induced-dipole field produced by the presence of the photoexcited electron−hole pair at times t = 0, 0.1, 1.7, 2.0, 3.3, and 5 ps, in correspondence with the charge dynamics shown in Figure 3. Unpolarized atoms are colored red, and the very polarized atoms are depicted in blue, with white atoms in between.

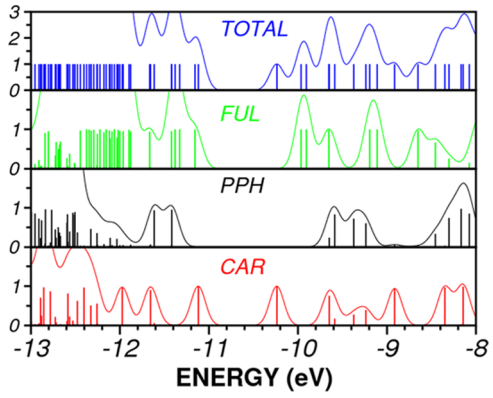

Figure 6. Density of states (DOS) for the triad, calculated for the molecular conformation at t = 0. The highest occupied molecular orbital (HOMO) of the triad lies at −11.12 eV. From top to bottom, the graphs show the total DOS (blue) and its projection on the FUL (green), PPH (black), and CAR (red) moieties.

orbitals of the PPH and CAR moieties cause the earliest electronic transfer to the carotenoid. However, such couplings evolve in time as a consequence of the electronic and the nuclear dynamics. That can be realized in Figure 7, where it is shown, on the left, the time evolution of the energy for some molecular orbitals. The highlighted curves (red, green, and black, according to the color code defined in Figure 1B) evince MOs that show a strong correlation with the electronic dynamics during the charge-separation event. On the right, the corresponding orbitals, calculated at t = 0. The behavior of the featured orbitals enlightens the mechanism that causes the electronic charge transfer to the FUL moiety at ∼2 ps—more about the electron localization is provided as Supporting Information. The self-trapping of the electron wavepacket, which is driven by the nonlinear polarizable Hückel Hamiltonian, starts to occur when the nonlinearity parameter increases above a critical value, as observed around 2 ps. In that regime, the meanfield component of the energy—the polarizability energy—produces strong shifts on the energies of

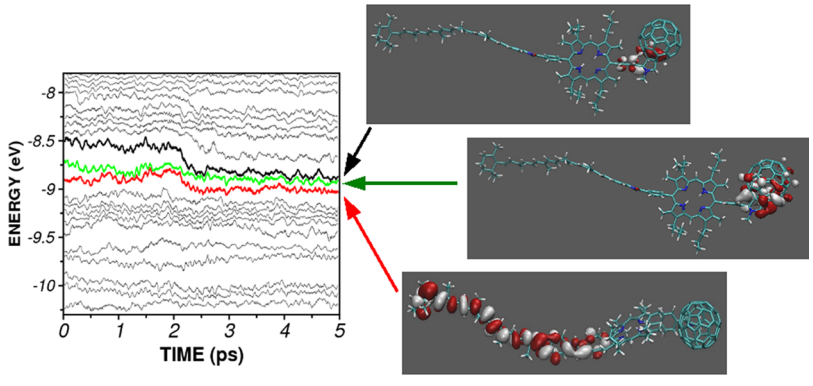

Figure 7. Panel shows, on the left, the time evolution of the energies of unoccupied molecular orbitals (MOs) upon which the wavepackets are propagated. In colors (red, green, and black, according to the color code defined in Figure 1B), we evince the MOs that show the strongest correlation with the electronic dynamics during the charge-separation event. On the right, the corresponding orbitals, calculated at t = 0.

dx.doi.org/10.1021/jp408955e | J. Phys. Chem. C 2014, 118, 126−134

some eigenmodes of the extended Hückel Hamiltonian. Such energy shifts promote charge transfer by the alignment of MOs localized on each of the fragments, thus, favoring the self-trapping effect. In this mechanism, the PPH moiety acts as a bridge that connects the CAR and FUL fragments. As the amount of charge transferred increases, the localized induced-dipole builds up. By analyzing the time-dependent pair-correlation functions for the occupation probabilities on the fragments that comprise the triad (Supporting Information), it is evident that fragments CAR and PPH transfer electronic charge to the FUL fragment. The carotenoid moiety functions as a secondary electron donor. In this respect, the temperature acts against the charge localization because the thermal fluctuations of the molecule tend to distribute the charge density of the wavepackets throughout the triad, whereas the self-trapping mechanism stabilizes the system by producing localized dipole moments between the fragments junctions. However, thermal fluctuations can still assist the charge-separation process by taking the charge distribution out of metastable energy minima, into more stable charge-separated states.

We also performed MD simulations for another kind of triad, composed of a *meso*-tetraaryl porphyrin, shown in Figure 8, and

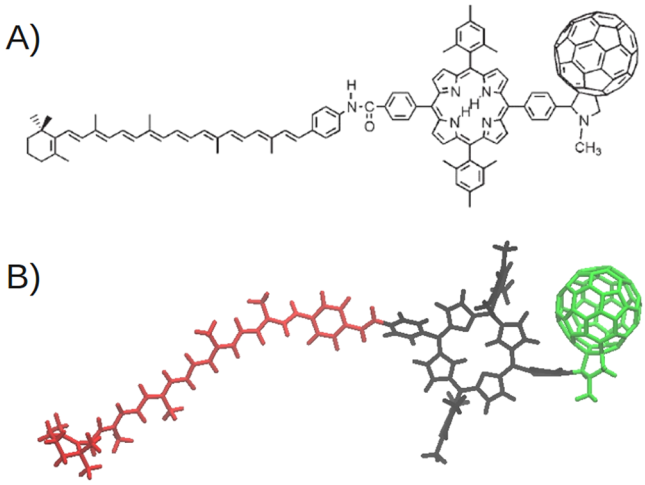

Figure 8. (A) Chemical structure of the $C-P-C_{60}$ triad formed by meso-substituted tetraaryl porphyrin. B) Typical geometry configuration obtained after MD thermalization in gas phase at 300 K.

we verified that such structures are appreciably more flexible than those previously discussed that consisted of the diaryl-octaalkyl-porphyrin (Figure 1). The most evident deformation modes in the MD trajectories are the saddle and ruffle distortions.[54,55] Quantum dynamics (QD) simulations were also carried out for this model system (see Figure 9) following the theoretical methods previously described. The electron was initially assigned to the LUMO and the hole to the HOMO of the PPH moiety (results for different wavepacket setups are included as Supporting Information). The QD simulations showed that the charge separation is less robust for the *meso*-tetraaryl-porphyrin triad, which we ascribe to the enhanced flexural and torsional modes of the macrocycle: the energy fluctuations produced by the wider nuclear thermal motion disrupt the MO alignments that promote the electronic self-trapping. From the experimental viewpoint, photochemical investigations indicate that the first charge-separation event in *meso*-aryl porphyrin triads takes longer ($\tau \sim 20-40$ ps[2,20]) than

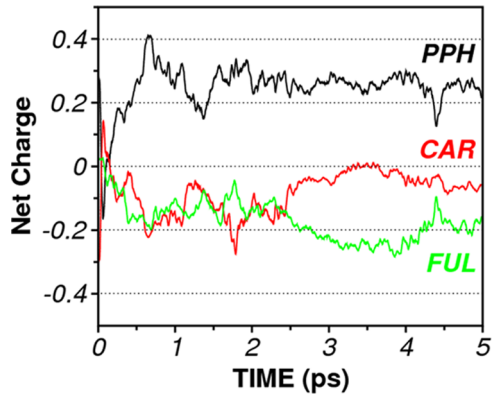

Figure 9. Time-dependent electron−hole net charge on each of the triad fragments: carotene (CAR, in red), porphyrin (PPH, in black), and fullerene (FUL, in green).

the β-substituted alkyl porphyrin triads (3 ps $< \tau <$ 12 ps).[1,2,14,20,22,24]

4. CONCLUSIONS

We have used a semiempirical quantum dynamics propagation method to simulate the primary charge-separation event that produces the $C-P^{\bullet+}-C_{60}^{\bullet-}$ state in photoexcited carotenoid−porphyrin−fullerene triads. The paper introduces a phenomenological Hamiltonian that naturally describes the charge dynamics and charge separation in the supramolecular triad. Two dynamical regimes are revealed for the electron−hole pair: a transient oscillatory behavior and the nonlinear self-trapping regime. The first regime is established within 200 fs, as the electron and hole wavepackets initially bounded to the porphyrin chromophore delocalize throughout the triad. The study also enlightens the role played by the intramolecular polarizability on the charge-separation effect. The effects are described in the framework of the self-trapping nonlinear Schrödinger equation (NLSE), which is well-known for describing the self-trapping phenomena in condensed matter, nonlinear optics, and atomic systems. The self-trapping of the electron wavepacket is driven by the nonlinear polarizable Hückel Hamiltonian, and it starts to occur when the nonlinearity parameter increases above a critical value, as observed around 2 ps. In that regime, the meanfield component of the energy—the polarizability energy—leads some of the eigenmodes into alignment, favoring the interfragment charge transfer and the self-trapping. Quantum dynamics simulations were performed for $C-P-C_{60}$ triads comprised of porphyrins with different side groups—β-alkyl and *meso*-aryl substituents. Although charge separation tends to occur for both structures, the effect occurs with less efficiency as the macrocycle becomes more flexible, as in the case of meso-substituted-tetraaryl porphyrins. On the basis of the simulation results, we ascribe the irreversible charge transfer, driven by the self-trapping effect, to the decay of the photoexcited state $C-{}^1P-C_{60}$ and the formation of the metastable charge-separated state $C-P^{\bullet+}-C_{60}^{\bullet-}$ that is measured in the photochemical experiments with picosecond time resolution.[1,2,14,15,20,21] In addition, we believe that the high time-resolution pump−probe differential transmission spectra obtained for time delays $t <$ 300 fs of the probe[25,58]—in particular, the transient photobleaching signal centered around the Q-band absorption resonance of the porphyrin moiety—can be associated to the initial charge delocalization effect.

dx.doi.org/10.1021/jp408955e | J. Phys. Chem. C 2014, 118, 126−134

■ ASSOCIATED CONTENT

Supporting Information

Includes a movie of the polarization dynamics shown in Figure 5, and also calculations of the excitation spectrum of the triad; summary about the nonlinear Schrödinger equation (NLSE); quantum dynamics calculations for different wavepacket initial conditions; analysis of time-dependent pair-correlation functions for the occupation probabilities for the electron and hole wavepackets. This material is available free of charge via the Internet at http://pubs.acs.org.

■ AUTHOR INFORMATION

Notes

The authors declare no competing financial interest.

■ ACKNOWLEDGMENTS

The authors are indebted to the Brazilian National Counsel of Technological and Scientific Development (CNPq) and the Coordenação de Aperfeiçoamento de Pessoal de Nível Superior for funding the project.

■ REFERENCES

(1) Gust, D.; Moore, T. A.; Moore, A. L. Mimicking Photosynthetic Solar Energy Transduction. *Acc. Chem. Res.* **2001**, *34*, 40−48.
(2) Kodis, G.; Liddell, P. A.; Moore, A. L.; Moore, T. A.; Gust, D. Synthesis and Photochemistry of a Carotene−Porphyrin−Fullerene Model Photosynthetic Reaction Center. *J. Phys. Org. Chem.* **2004**, *17*, 724−734.
(3) Holten, D.; Bocian, D. F.; Lindsey, J. S. Probing Electronic Communication in Covalently Linked Multiporphyrin Arrays. A Guide to the Rational Design of Molecular Photonic Devices. *Acc. Chem. Res.* **2002**, *35*, 57−69.
(4) Scholes, G. D.; Fleming, G. R.; Olaya-Castro, A.; van Grondelle, R. Lessons from Nature About Solar Light Harvesting. *Nat. Chem.* **2011**, *3*, 763−774.
(5) McConnell, I.; Li, G.; Brudvig, G. Energy Conversion in Natural and Artificial Photosynthesis. *Chem. Biol. Rev.* **2010**, *17*, 434−437.
(6) Scholes, G. D.; Mirkovic, T.; Turner, D. B.; Fassioli, F.; Buchleitner, A. Solar Light Harvesting by Energy Transfer: From Ecology to Coherence. *Energy Environ. Sci.* **2012**, *5*, 9374−9393.
(7) Blankenship, R. E.; Tiede, D. M.; Barber, J.; Brudvig, G. W.; Fleming, G.; Ghirardi, M.; Gunner, M. R.; Junge, W.; Kramer, D. M.; Melis, A.; et al. Comparing Photosynthetic and Photovoltaic Efficiencies and Recognizing the Potential for Improvement. *Science* **2011**, *332*, 805−809.
(8) Gust, D.; Moore, T. A.; Moore, A. L. Solar Fuels via Artificial Photosynthesis. *Acc. Chem. Res.* **2009**, *42*, 1890−1898.
(9) Clarke, T. M.; Durrant, J. Charge Photogeneration in Organic Solar Cells. *Chem. Rev.* **2010**, *110*, 6736−6767.
(10) Hardin, B. E.; Snaith, H. J.; McGehee, M. D. The Renaissance of Dye-Sensitized Solar Cells. *Nat. Photonics* **2012**, *6*, 162−169.
(11) Holten, D.; Windsor, M. W. Picosecond Flash Photolysis in Biology and Biophysics. *Annu. Rev. Biophys. Bioeng.* **1978**, *7*, 189−227.
(12) Beddard, G. S.; Porter, G.; Tredwell, C. J.; Barber, J. Fluorescence Lifetimes in the Photosynthetic Unit. *Nature* **1975**, *258*, 166−168.
(13) Shapiro, S. L.; Auston, D. H. *Ultrashort Light Pulses: Picosecond Techniques and Applications*; Springer-Verlag: Berlin, 1984.
(14) Kuciauskas, D.; Liddell, P. A.; Lin, S.; Johnson, T. E.; Weghorn, S. J.; Lindsey, J. S.; Moore, A. L.; Moore, T. A.; Gust, D. An Artificial Photosynthetic Antenna-Reaction Center Complex. *J. Am. Chem. Soc.* **1999**, *121*, 8604−8614.
(15) D'Souza, F.; Chitta, R.; Ohkubo, K.; Tasior, M.; Subbaiyan, N. K.; Zandler, M. E.; Rogacki, M. K.; Gryko, D. T.; Fukuzumi, S. Corrole−Fullerene Dyads: Formation of Long-Lived Charge-Separated States in Non-Polar Solvents. *J. Am. Chem. Soc.* **2008**, *130*, 14263−14272.
(16) Buruah, T.; Pederson, M. R. Density Functional Study on a Light-Harvesting Carotenoid−Porphyrin−C_{60} Molecular Triad. *J. Chem. Phys.* **2006**, *125*, 164706−5.
(17) Buruah, T.; Pederson, M. R. DFT Calculations on Charge-Transfer States of a Carotenoid−Porphyrin−C_{60} Molecular Triad. *J. Chem. Theor. Comp.* **2009**, *5*, 834−843.
(18) Spallanzani, N.; Rozzi, C. A.; Varsano, D.; Baruah, T.; Pederson, M. R.; Manghi, F.; Rubio, A. Photoexcitation of a Light-Harvesting Supramolecular Triad: A Time-Dependent DFT Study. *J. Phys. Chem. B Lett.* **2009**, *113*, 5345−5349.
(19) Su, G.; Czader, A.; Homouz, D.; Bernardes, G.; Mateen, S.; Cheung, M. S. Multiscale Simulation on a Light-Harvesting Molecular Triad. *J. Phys. Chem. B* **2011**, *116*, 8460−8473.
(20) Kodis, G.; Liddell, P. A.; de la Garza, L.; Clausen, P. C.; Lindsey, J. S.; Moore, A. L.; Moore, T. A.; Gust, D. Efficient Energy Transfer and Electron Transfer in an Artificial Photosynthetic Antenna-Reaction Center Complex. *J. Phys. Chem. A* **2002**, *106*, 2036−2048.
(21) Kahnt, A.; Kärnbratt, J.; Esdaile, L. J.; Hutin, M.; Sawada, K.; Anderson, H. L.; Albinsson, B. Temperature Dependence of Charge Separation and Recombination in Porphyrin Oligomer−Fullerene Donor−Acceptor Systems. *J. Am. Chem. Soc.* **2011**, *133*, 9863−9871.
(22) Liddell, P. A.; Kuciauskas, D.; Sumida, J. P.; Nash, B.; Nguyen, D.; Moore, A. L.; Moore, T. A.; Gust, D. Photoinduced Charge Separation and Charge Recombination to a Triplet State in a Carotene−Porphyrin−Fullerene Triad. *J. Am. Chem. Soc.* **1997**, *119*, 1400−1405.
(23) Gust, D.; Moore, T. A.; Moore, A. L.; Kuciauskas, D.; Liddell, P. A.; Halbert, B. D. Mimicry of Carotenoid Photoprotection in Artificial Photosynthetic Reaction Centers: Triplet-Triplet Energy Transfer by a Relay Mechanism. *J. Photochem. Photobiol.* **1998**, *43*, 209−216.
(24) Kuciauskas, D.; Liddell, P. A.; Lin, S.; Stone, S. G.; Moore, A. L.; Moore, T. A.; Gust, D. Photoinduced Electron Transfer in Carrotenoporphyrin−Fullerene Triads: Temperature and Solvent Effects. *J. Phys. Chem. B* **2000**, *104*, 4307−4321.
(25) Rozzi, C. A.; Falke, S. M.; Spallanzani, N.; Rubio, A.; Molinari, E.; Brida, D.; Maiuri, M.; Cerullo, G.; Schramm, H.; Christoffers, J.; Lienau, C. Quantum Coherence Controls the Charge Separation in a Prototypical Artificial Light-Harvesting System. *Nat. Commun.* **2013**, *4*, 1602−1607.
(26) May, V.; Kühn, O. *Charge and Energy Transfer Dynamics in Molecular Systems*; WILEY-VCHVerlag GmBH & Co.: Weinheim, Germany, 2011.
(27) Nitzan, A. *Chemical Dynamics in Condensed Phases: Relaxation, Transfer, and Reactions in Condensed Molecular Systems*; Oxford university Press: Oxford, U.K., 2006.
(28) Albiez, M.; Gati, R.; Fölling, J.; Hunsmann, S.; Cristiani, M.; Oberthaler, M. K. Direct Observation of Tunneling and Nonlinear Self-Trapping in a Single Bosonic Josephson Junction. *Phys. Rev. Lett.* **2005**, *95*, 010402.
(29) D'Agosta, R.; Presilla, C. States Without a Linear Counterpart in Bose−Einstein Condensates. *Phys. Rev. A* **2002**, *65*, 043609.
(30) Smerzi, A.; Fantoni, S.; Giovanazzi, S.; Shenoy, S. R. Quantum Coherent Atomic Tunneling between Two Trapped Bose-Einstein Condensates. *Phys. Rev. Lett.* **1997**, *79*, 4950.
(31) Ostrovskaya, E. A.; Kivshar, Y. S.; Lisak, M.; Hall, B.; Cattani, F.; Anderson, D. Coupled-Mode Theory for Bose−Einstein Condensates. *Phys. Rev. A* **2000**, *61*, 031601.
(32) Hasegawa, A.; Matsumoto, M. *Optical Solitons in Fibers*; Springer: Berlin, 2003.
(33) Kenkre, V. M.; Campbell, D. K. Self-Trapping on a Dimer: Time-Dependent Solutions of a Discrete Nonlinear Schrödinger Equation. *Phys. Rev. B* **1986**, *34*, 4959.
(34) Eilbeck, J. A.; Lomdahl, P. S.; Scott, A. C. The Discrete Self-Trapping Equation. *Physica D* **1985**, *16*, 318−338.
(35) Feddersen, H. Localization of Vibrational Energy in Globular Protein. *Phys. Lett. A* **1991**, *154*, 391−395.

(36) *Nonlinearity in Condensed Matter—Springer Series in Solid-State Sciences*; Bishop, A. R., Campbell, D. K., Trullinger, S. E., Kumar, P., Eds.; Springer: New York, 1987; Vol. *69*.
(37) Turner, D. B.; Wilk, K. E.; Curmi, P. M. G.; Scholes, G. D. Comparison of Electronic and Vibrational Coherence Measured by Two-Dimensional Electronic Spectroscopy. *J. Phys. Chem. Lett.* **2011**, *2*, 1904−1911.
(38) Hoff, D. A.; da Silva, R.; Rego, L. G. C. Subpicosecond Dynamics of Metal-to-Ligand Charge-Transfer Excited States in Solvated $(Ru(bpy)_3)^{2+}$ Complexes. *J. Phys. Chem. C* **2011**, *115*, 15617−15626.
(39) Hoff, D. A.; da Silva, R.; Rego, L. G. C. Coupled Electron-Hole Quantum Dynamics on D-π-A Dye-Sensitized TiO_2 Semiconductors. *J. Phys. Chem. C* **2012**, *116*, 21169−21178.
(40) Abuabara, S. G.; Rego, L. G. C.; Batista, V. S. Influence of Thermal Fluctuations on Interfacial Electron Transfer in Functionalized TiO_2 Semiconductors. *J. Am. Chem. Soc.* **2005**, *127*, 18234−18242.
(41) Seifert, G.; Porezag, D.; Frauenheim, T. Calculations of Molecules, Clusters, and Solids with a Simplified LCAO-DFT-LDA Scheme. *Int. J. Quantum Chem.* **1996**, *58*, 185−192.
(42) Porezag, D.; Frauenheim, T.; Köhler, T.; Seifert, G.; Kaschner, R. Construction of Tight-Binding-Like Potentials on the Basis of Density-Functional Theory: Application to Carbon. *Phys. Rev. B* **1995**, *51*, 12947−12957.
(43) Seifert, G.; Joswig, J.-O. Density-Functional Tight Binding: An Approximate Density-Functional Theory Method. *WIREs Comput. Mol. Sci.* **2012**, *2*, 456−465.
(44) Elstner, M.; Porezag, D.; Jungnickel, G.; Elsner, J.; Haugk, M.; Frauenheim, T.; Suhai, S.; Seifert, G. Self-Consistent-Charge Density-Functional Tight-Binding Method for Simulations of Complex Materials Properties. *Phys. Rev. B* **1998**, *58*, 7260−7628.
(45) Niehaus, T. A.; Suhai, S.; Della Sala, F.; Lugli, P.; Elstner, M.; Seifert, G.; Frauenheim, T. Tight-Binding Approach to Time-Dependent Density-Functional Response Theory. *Phys. Rev. B* **2001**, *63*, 085108−085109.
(46) McGlynn, S. P.; Vanquickenborne, L. G.; Kinoshita, M.; Carroll, D. G. *Introduction to Applied Quantum Chemistry*; Holt, Rinehart and Winston, Inc..: New York, 1972.
(47) da Silva, R.; Rego, L. G. C.; Freire, J. A.; Rodriguez, J.; Laria, D.; Batista, V. S. Study of Redox Species and Oxygen Vacancy Defects at TiO_2-Electrolyte Interfaces. *J. Am. Chem. Soc.* **2010**, *114*, 19433−19442.
(48) $K_{ij} = k_{WH} + \Delta^2 + \Delta^4(1 - k_{WH})$, where $k_{WH} = (k_i + k_j)/2$ and $\Delta = (E_i - E_j)/(E_i + E_j)$, $k_i = 1.75$ provides a good description for the CAR and FUL moieties, whereas $k_i = 2.05$ is used just for the carbon atoms of the PPH. Ammeter, J. H.; Buergi, H. B.; Thibeault, J. C.; Hoffmann, R. Counterintuitive Orbital Mixing in Semiempirical and Ab Initio Molecular orbital Calculation. *J. Am. Chem. Soc.* **1978**, *100*, 3686−3692.
(49) *CRC Handbook of Chemistry and Physics*, 85th ed; Lide, D. R., Ed.; CRC Press: Boca Raton, FL, 2005.
(50) Hoff, D. A.; Rego, L. G. C. In *Specialist Periodical Reports—Chemical Modelling: Modelling Electron Quantum Dynamics in Large Molecular Systems*; Springboard, M., Joswig, J.-O., Eds.; RSC Publishing: London, 2013; Vol. *10*, pp 102−126.
(51) Rizzi, A. C.; van Gastel, M.; Liddell, P. A.; Palacios, R. E.; Moore, G. F.; Kodis, G.; Moore, A. L.; Moore, T. A.; Gust, D.; Braslavsky, S. E. Entropic Changes Control the Charge Separation Process in Triads Mimicking Photosynthetic Charge Separation. *J. Phys. Chem. A* **2008**, *112*, 4215−4223.
(52) Guldi, D. M. Fullerene−Porphyrin Architectures; Photosynthetic Antenna and Reaction Center Models. *Chem. Soc. Rev.* **2002**, *31*, 22−36.
(53) Nurco, D. J; Medforth, J.; Forsyth, T. P.; Olmstead, M. M.; Smith, K. M. Conformational Flexibility in Dodecasubstituted Porphyrins. *J. Am. Chem. Soc.* **1996**, *118*, 10918−10919.
(54) Haddad, R. E.; Gazeau, S.; Pécaut, J.; Marchon, J.-C.; Medforth, G. J.; Shelnutt, J. A. Origin of the Red Shifts in the Optical Absorption Bands of Nonplanar Tetraalkylporphyrins. *J. Am. Chem. Soc.* **2003**, *125*, 1253−1268.
(55) Senge, M. O. Exercises in Molecular Gymnastics-Bending, Stretching and Twisting Porphyrins. *Chem. Commun.* **2006**, *3*, 243−256.
(56) Zakavi, S.; Omidyan, R.; Ebrahimi, L.; Heidarizadi, F. Substitution Effects on the UV−Vis and 1H NMR Spectra of the Dications of Meso and/or β Substituted Porphyrins with Trifluoroacetic Acid: Electron-Deficient Porphyrins Compared to the Electron-Rich Ones. *Inorg. Chem. Commun.* **2011**, *14*, 1827−1832.
(57) Rosa, A.; Ricciardi, G.; Baerends, E. J. Synergism of Porphyrin-Core Saddling and Twisting of *Meso*-Aryl Substituents. *J. Phys. Chem. A* **2006**, *110*, 5180−5190.
(58) Rozzi, C. A.; Falke, S. M.; Spallanzani, N.; Rubio, A.; Molinari, E.; Brida, D.; Maiuri, M.; Cerullo, G.; Schramm, H.; Christoffers, J.; Lienau, C. Quantum Coherence Controls the Charge Separation in a Prototypical Artificial Light-Harvesting System. *Nat. Commun.* **2013**, *4*, 1602/1−1602/7 Supplementary Information, Supplementary Figures S1-S7.